Nonlocal energetic particle mode in a JT-60U plasma

Y. Todo
National Institute for Fusion Science, Toki, Gifu 509-5292, Japan

K. Shinohara, M. Takechi, and M. Ishikawa
Naka Fusion Research Establishment, Japan Atomic Energy Research Institute, Naka, Ibaraki 311-0193, Japan

(Received 20 July 2004; accepted 12 October 2004; published online 3 December 2004)

Energetic-ion driven instability in a Japan Atomic Energy Research Institute Tokamak-60 Upgrade (JT-60U) [S. Ishida *et al.*, Phys. Plasmas **11**, 2532 (2004)] plasma was investigated using a simulation code for magnetohydrodynamics and energetic particles. The spatial profile of the unstable mode peaks near the plasma center where the safety factor profile is flat. The unstable mode is not a toroidal Alfvén eigenmode (TAE) because the spatial profile deviates from the expected location of TAE and the spatial profile consists of a single primary harmonic $m/n=2/1$ where m and n are poloidal and toroidal mode numbers. The real frequency of the unstable mode is close to the experimental starting frequency of the fast frequency sweeping mode. Simulation results demonstrate that energetic-ion orbit width and energetic-ion pressure significantly broaden radial profile of the unstable mode. For the smallest value among the investigated energetic-ion orbit width, the unstable mode is localized within 20% of the minor radius. This gives an upper limit of the spatial profile width of the unstable mode which the magnetohydrodynamic effects alone can induce. For the experimental condition of the JT-60U plasma, energetic ions broaden the radial width of the unstable mode spatial profile by a factor of 3. The unstable mode is primarily induced by the energetic particles. © *2005 American Institute of Physics*. [DOI: 10.1063/1.1828084]

I. INTRODUCTION

Three types of frequency chirping instabilities, slow frequency sweeping (slow FS) mode, fast frequency sweeping (fast FS) mode, and abrupt large event (ALE) have been observed in the Japan Atomic Energy Research Institute Tokamak-60 Upgrade (JT-60U) (Ref. 1) plasmas heated with negative ion based neutral beam (NNB) injection.[2–5] Frequencies of the three instabilities are in the range of shear Alfvén eigenmodes. Frequency sweeping of slow FS mode has a good correlation with equilibrium parameter evolution with time scale $\simeq$200 ms. On the other hand, time scales of the fast FS mode and the ALE are, respectively 1–5 ms and 200–400 μs, much shorter than the equilibrium time scale. Frequency of the fast FS mode shifts rapidly by 10–20 kHz in 1–5 ms both upward and downward. The starting frequency of the fast FS mode changes in the time scale of the equilibrium parameter evolution and follows the toroidal Alfvén eigenmode (TAE) (Refs. 6 and 7) gap frequency.

We have previously investigated the fast FS mode in a JT-60U plasma using a simulation code for magnetohydrodynamics (MHD) and energetic particles, MEGA.[8] We reported that there is an unstable mode near the plasma center and frequency sweeping close to that of the fast FS mode takes place.[9] The ratio of the linear damping rate γ_d to the linear growth rate γ_L in the simulation is consistent with hole-clump pair creation which takes place when γ_d/γ_L is greater than 0.4.[10,11]

In this paper, we focus on the linear properties of the unstable mode. In Ref. 9, we called the unstable mode "nonlocal energetic particle mode (EPM)" and argued that it is different from the resonant type EPM (Refs. 12 and 13) and similar to the EPM which is predicted for ICRF heated plasma with reversed magnetic shear.[14,15] However, it was shown numerically that the reversed-shear-induced Alfvén eigenmode,[16] which has properties similar to the global Alfvén eigenmode,[17] can exist in reversed shear plasmas. It was demonstrated that MHD theory can explain frequency chirping behavior of so-called Alfvén cascades observed in reversed shear plasmas.[18–20] Recently, the α particle driven Alfvén eigenmode observed in the Tokamak fusion test reactor was reexamined and explained in terms of the cylindrical-like MHD eigenmode.[21] In Ref. 22 it is theoretically clarified that both toroidal MHD effects of second order in inverse aspect ratio and adiabatic response of energetic particles can establish an eigenmode localized near the magnetic surface where the safety factor takes the minimum value in reversed shear plasmas. Furthermore, it is pointed out that the eigenmode equation, Eq. (22) in Ref. 22 is valid also for positive magnetic shear plasma if magnetic shear is sufficiently weak.[22] This gives us a new viewpoint to investigate linear properties of the unstable mode which we reported in Ref. 9.

The energetic-ion terms in the eigenmode equation, Eq. (22) in Ref. 22 were derived in Ref. 14 under an assumption that the grad-B and curvature drift term dominates over the time derivative term and the parallel velocity term in the linearized Vlasov equation. It is not clear whether the assumption is valid for passing energetic ions in the JT-60U plasma heated with NNB injection. It is worthwhile investigating whether energetic-ion orbit width and energetic-ion pressure have significant effects on spatial profile of the unstable mode found in Ref. 9. Another interesting question is whether there exists a MHD eigenmode in the limit of the

smallest energetic-ion orbit width or the lowest energetic-ion pressure. Investigation for the limit cases is needed, although instability growth rate is low in the limit cases and we cannot investigate stable modes with the initial value approach. We have carried out simulations for various energetic-ion orbit width and energetic-ion pressure using the MEGA code and found that they have significant effects on spatial profile of the unstable mode in the JT-60U plasma. We have analyzed restoring force of the unstable mode and found that energetic ions have a significant contribution in restoring force to broaden spatial profile of the unstable mode. We describe simulation model and method in Sec. II. Section III is devoted to simulation results. Summary is given in Sec. IV.

II. SIMULATION MODEL

The hybrid simulation model for MHD and energetic particles[23,24,8] is employed in the MEGA code. Plasma is divided into bulk plasma and energetic ions. The bulk plasma is described by the nonlinear full MHD equations. Electromagnetic field is given by the MHD description. This approximation is reasonable under the condition that the energetic-ion density is much less than the bulk plasma density. The MHD equations with energetic-ion effects are

$$\frac{\partial \rho}{\partial t} = -\nabla \cdot (\rho \mathbf{v}), \tag{1}$$

$$\rho \frac{\partial}{\partial t}\mathbf{v} = -\rho\omega \times \mathbf{v} - \rho \nabla \left(\frac{v^2}{2}\right) - \nabla p + (\mathbf{j} - \mathbf{j}_h) \times \mathbf{B} - \nu\rho \nabla \times \omega + \tfrac{4}{3}\nu\rho \nabla (\nabla \cdot \mathbf{v}), \tag{2}$$

$$\frac{\partial \mathbf{B}}{\partial t} = -\nabla \times \mathbf{E}, \tag{3}$$

$$\frac{\partial p}{\partial t} = -\nabla \cdot (p\mathbf{v}) - (\gamma - 1)p \nabla \cdot \mathbf{v} + (\gamma - 1)\left[\nu\rho\omega^2 + \tfrac{4}{3}\nu\rho(\nabla \cdot \mathbf{v})^2 + \eta j^2\right], \tag{4}$$

$$\mathbf{E} = -\mathbf{v} \times \mathbf{B} + \eta \mathbf{j}, \tag{5}$$

$$\boldsymbol{\omega} = \nabla \times \mathbf{v}, \tag{6}$$

$$\mathbf{j} = \frac{1}{\mu_0} \nabla \times \mathbf{B}, \tag{7}$$

where μ_0 is the vacuum magnetic permeability and γ is the adiabatic constant, and all the other quantities are conventional. Here, $\mathbf{j}_h$ is the energetic ion current density without $\mathbf{E} \times \mathbf{B}$ drift. In the simulations reported in this paper, wet set $\nu = \eta = 0$. The effect of the energetic ions on the MHD fluid is taken into account in the MHD momentum equation [Eq. (2)] through the energetic-ion current. The MHD equations are solved using a finite difference scheme of fourth-order accuracy in space and time.

The drift-kinetic description is employed for the energetic ions. The guiding-center velocity $\mathbf{u}$ is given by

$$\mathbf{u} = \mathbf{v}_{\parallel}^{*} + \mathbf{v}_E + \mathbf{v}_B, \tag{8}$$

$$\mathbf{v}_{\parallel}^{*} = \frac{v_{\parallel}}{B^*}[\mathbf{B} + \rho_{\parallel} B \nabla \times \mathbf{b}], \tag{9}$$

$$\mathbf{v}_E = \frac{1}{B^*}[\mathbf{E} \times \mathbf{b}], \tag{10}$$

$$\mathbf{v}_B = \frac{1}{q_h B^*}[-\mu \nabla B \times \mathbf{b}], \tag{11}$$

$$\rho_{\parallel} = \frac{m_h v_{\parallel}}{q_h B}, \tag{12}$$

$$\mathbf{b} = \mathbf{B}/B, \tag{13}$$

$$B^* = B(1 + \rho_{\parallel} \mathbf{b} \cdot \nabla \times \mathbf{b}), \tag{14}$$

$$m_h v_{\parallel} \frac{dv_{\parallel}}{dt} = \mathbf{v}_{\parallel}^{*} \cdot [q_h \mathbf{E} - \mu \nabla B], \tag{15}$$

where $v_{\parallel}$ is the velocity parallel to the magnetic field, μ is the magnetic moment which is the adiabatic invariant, and m_h and q_h are energetic ion mass and electric charge. The energetic ion current density without $\mathbf{E} \times \mathbf{B}$ drift in Eq. (2) is

$$\mathbf{j}_h = \int (\mathbf{v}_{\parallel}^{*} + \mathbf{v}_B) f d^3v - \nabla \times \int \mu \mathbf{b} f d^3v, \tag{16}$$

where the second term in the right-hand side is the magnetization current. The $\mathbf{E} \times \mathbf{B}$ drift $\mathbf{v}_E$ disappears in $\mathbf{j}_h$ due to quasineutrality.[8]

It is important to start simulation from MHD equilibrium consistent with energetic-ion distribution. When the energetic-ion pressure is isotropic in the velocity space, the energetic-ion contribution in Eq. (2) is just a scalar pressure gradient in the same form as the bulk pressure gradient.[8] Then, the equilibrium can be obtained from the Grad–Shafranov equation neglecting the energetic-ion orbit width. However, if the energetic-ion pressure is anisotropic in the velocity space and/or the energetic-ion orbit width is not negligibly small, the Grad–Shafranov equation should be extended. We solve an extended Grad–Shafranov equation developed in Ref. 25 in the cylindrical coordinates (R, φ, z) where R is the major radius coordinate, φ is the toroidal angle coordinate, and z is the vertical coordinate. Let us start by expressing initial energetic-ion distribution as a function of toroidal canonical momentum P_{φ}, kinetic energy ϵ, and magnetic moment μ,

$$f_0 = f_0(P_{\varphi}, \epsilon, \mu) \tag{17}$$

where the subscript 0 denotes initial value. Since f_0 is a function of invariants in axisymmetric plasmas without electric field, it is an equilibrium distribution. Using the equilibrium distribution function, the energetic-ion current density is given by

$$\mathbf{j}_h = \int q_h(\mathbf{v}_\parallel^* + \mathbf{v}_B) f_0(P_\varphi, \epsilon, \mu) d^3v - \nabla \times \int \mu f_0(P_\varphi, \epsilon, \mu) \mathbf{b} d^3v. \quad (18)$$

Note that $\nabla \cdot \mathbf{j}_h = 0$ is satisfied because we have steady energetic-ion density with the equilibrium distribution. Then, energetic-ion poloidal current density can be expressed using a stream function K in axisymmetric system,

$$j_{h_R} = -\frac{1}{R}\frac{\partial K}{\partial z}, \quad (19)$$

$$j_{h_z} = \frac{1}{R}\frac{\partial K}{\partial R}. \quad (20)$$

Using the stream function K the extended Grad–Shafranov equation is given by[25]

$$R\frac{\partial}{\partial R}\frac{1}{R}\frac{\partial \psi}{\partial R} + \frac{\partial^2 \psi}{\partial z^2} = -\mu_0 R^2 \frac{d}{d\psi} p - \mu_0 R j_{h_\varphi} - \frac{I}{(2\pi)^2}\frac{dM}{d\psi}, \quad (21)$$

$$I \equiv 2\pi R B_\varphi, \quad (22)$$

$$M \equiv I - 2\pi K, \quad (23)$$

where ψ is the poloidal magnetic flux. Note that M depends only on ψ while both I and K depend on ψ and the poloidal angle.

Equation (21) is coupled with Eqs. (18)–(20) and solved by numerical iteration. The safety factor q profile, bulk pressure profile, energetic ion pressure profile, and parameters of energetic ion distribution $f_0(P_\varphi, \epsilon, \mu)$ are specified before iteration. In the simulations reported in this paper, we neglect energetic-ion velocity perpendicular to magnetic field because the NNB injection in the JT-60U experiment was tangential. We assume energetic-ion distribution in the form

$$f_0(P_\varphi, \epsilon, \mu) = \sum_{l=0}^{L} a_l \left(\frac{P_{\varphi_{max}} - P_\varphi}{P_{\varphi_{max}} - P_{\varphi_{min}}}\right)^l \frac{1}{\epsilon^{3/2} + \epsilon_c^{3/2}} \frac{1}{2}\left[1 - \tanh\left(\frac{\epsilon^{1/2} - \epsilon_b^{1/2}}{(\Delta\epsilon)^{1/2}}\right)\right] \delta(\mu). \quad (24)$$

Here, a_l is chosen at each iteration step using the least square method so that

$$P_{h\parallel} = \int m_h v_\parallel^2 f_0(P_\varphi, \epsilon, \mu) d^3v \quad (25)$$

is close to the specified energetic-ion parallel pressure profile. We have chosen $L=5$ for numerical convergence. The parameters, ϵ_b is the NNB injection energy, ϵ_c is the critical energy above which the collisions with electrons dominates over those with ions, and $\Delta\epsilon$ is chosen to be $10^{-2}\epsilon_b$.

The δf method[26–28] is used for the energetic ions. The marker particles are initially loaded uniformly in the phase space. With the uniform loading employed in this work, the number of energetic beam ions that each marker particle represents is in proportion to the initial distribution function, namely, the particle density in the phase space. We introduce a normalization factor α which is chosen so that

$$\int P_{h\parallel 0} + 2P_{h\perp 0} dV = \alpha \sum_{i=1}^{N} [m_h v_{\parallel i}^2 + 2\mu_i B(\mathbf{x}_i)] f_0(P_{\varphi_i}, \epsilon_i, \mu_i) \quad (26)$$

is initially satisfied, where the subscript 0 denotes initial value and N is the total number of marker particles used.

Time evolution of each particle's weight is given by

$$\frac{d}{dt} w = -\alpha \left[\frac{dP_\varphi}{dt}\frac{\partial f_0}{\partial P_\varphi} + \frac{d\epsilon}{dt}\frac{\partial f_0}{\partial \epsilon}\right], \quad (27)$$

$$w(t=0) = 0. \quad (28)$$

The energetic-ion current $\mathbf{j}_h$ in Eq. (2) is calculated using the particle weight,

$$\mathbf{j}_h = \mathbf{j}_{h0} + \sum_{i=1}^{N} w_i q_h (\mathbf{v}_{\parallel i}^* + \mathbf{v}_{Bi}) S(\mathbf{x} - \mathbf{x}_i) - \nabla \times \left[\mathbf{b} \sum_{i=1}^{N} w_i \mu_i S(\mathbf{x} - \mathbf{x}_i)\right], \quad (29)$$

where $S(\mathbf{x} - \mathbf{x}_i)$ is the shape factor of marker particle.

The MEGA code is benchmarked with respect to the linear growth rate of the α-particle driven $n=4$ TAE in the TFTR D-T plasma shot No. 103101.[29] The initial energetic particle distribution is similar to that of a previous particle simulation reported in Ref. 30, where roughly an isotropic distribution for the energetic particles (which in this benchmark case were α particles) is used in the velocity space. The number of marker particles used is 5.2×10^5. The number of grid points is $101\times16\times101$ for the cylindrical coordinates (R, φ, z), where R is the major radius coordinate, φ is the toroidal angle coordinate, and z is the vertical coordinate. The simulation domain in the toroidal angle coordinate is $0<\varphi<\pi/2$ for this benchmark test of $n=4$ TAE. The destabilized mode has a TAE spatial profile which consists of two major harmonics $m/n=6, 7/4$ and frequency 215 kHz. These results are consistent with the calculation with the NOVA-K code.[31] The linear growth rate obtained from this simulation, is 8.7×10^{-3} of the mode frequency. This linear growth rate is close to what is observed in the previous particle simulation 1.1×10^{-2} (Ref. 30) and calculated in the NOVA-K code 8×10^{-3}.[31]

III. SIMULATION RESULTS

A. Instability in a JT-60U plasma

The JT-60U discharge E36379,[4] where the fast FS mode was observed, was investigated using the MEGA code. The safety factor profile, bulk pressure profile, and density profile used in the simulation are based on the experimental data. The major and minor radii are $R_0=3.4$ m and $a=1.0$ m, respectively. The shape of the outermost magnetic surface in the simulation is circular while it was diverter-shaped in the experiment. The magnetic field at the magnetic axis is 1.2 T. The bulk plasma and the beam ions are deuterium. NNB

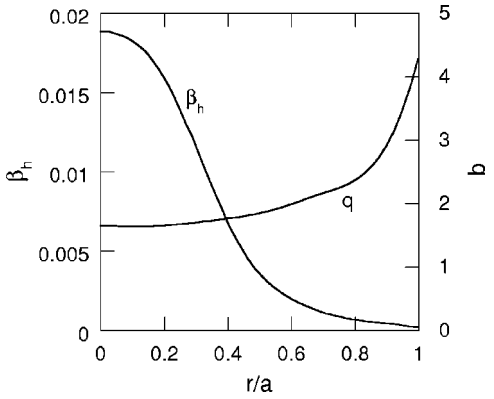

FIG. 1. Energetic-ion beta β_h profile and safety factor q profile.

injection energy is 346 keV. Initial energetic-ion distribution in the velocity space is assumed to be a slowing down distribution. Energetic-ion velocity perpendicular to magnetic field is neglected because the NNB injection is tangential. The beam direction is parallel to the plasma current. The maximum velocity is assumed to be 80% of the injection velocity as the injection is not completely parallel to the magnetic field. This maximum velocity in the simulation corresponds roughly to the Alfvén velocity at the magnetic axis. The number of marker particles used is 5.2×10^5. The number of grid points is $101\times16\times101$ for the cylindrical coordinates (R,φ,z), where R is the major radius coordinate, φ is the toroidal angle coordinate, and z is the vertical coordinate.

Linearly unstable mode was investigated for energetic-ion pressure profile based on a calculation using the OFMC code.[32] The OFMC code calculation gives classical distribution, which is established by NNB injection and particle collisions. Energetic-ion redistribution and loss due to ALE and fast FS mode is not considered in the OFMC code calculation. The energetic-ion pressure profile and q profile used in the simulation are shown in Fig. 1. The central β value is 1.9%. The ratio of energetic-ion parallel Larmor radius defined in Eq. (12) to the minor radius $\rho_{h\|}/a$ is 0.08. The energetic-ion parallel Larmor radius is calculated using the maximum energy ϵ_b in Eq. (24). An unstable mode was found with the TAE range of frequency. For data analysis magnetic flux surface coordinates (r,φ,θ) where r is the minor radius coordinate and θ is the poloidal angle coordinate are constructed. Spatial profile of the radial velocity v_r of the unstable mode is shown in Fig. 2. The primary harmonic is $m/n=2/1$, where m and n are poloidal and toroidal mode numbers. Phase in all of the figures of radial velocity profile in this paper are chosen so as to maximize the cosine part of the intensity of the $m/n=2/1$ harmonic. Figure 3 shows frequency and location of the unstable mode. The location of the unstable mode is defined by the region where total intensity of sine and cosine parts of the $m/n=2/1$ harmonic of radial velocity v_r is larger than 10% of the peak value. Frequency of the unstable mode is $0.25\omega_A$, where $\omega_A=v_A/R_0$ and v_A is the Alfvén velocity at the plasma center. The frequency corresponds to 52 kHz, which is close to the starting frequency of the fast FS mode. In Fig. 3 also shown are the $n=1$ shear Alfvén continuous spectra. The gap in the

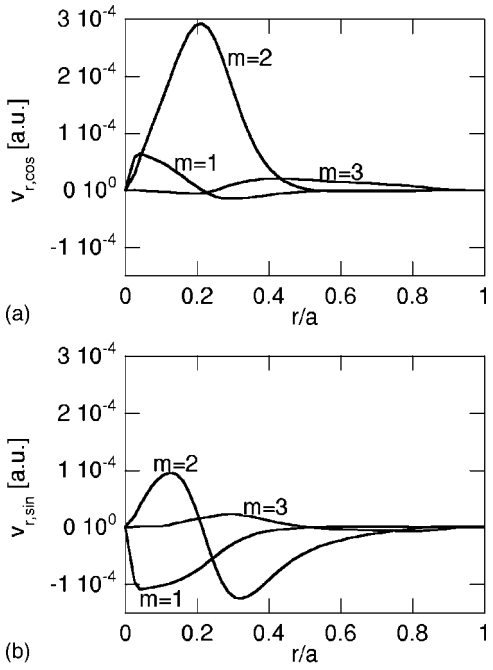

FIG. 2. Spatial profiles of (a) cosine part and (b) sine part of the unstable mode radial velocity v_r harmonics for $\rho_{h\|}/a=0.08$. Toroidal mode number of all the harmonics is $n=1$.

Alfvén continuous spectra at $q=2.5$ for $m/n=2,3/1$ harmonics is located at $r/a\sim0.8$. If the unstable mode is a TAE, it must be located at the gap $(r/a\sim0.8)$ and must consist of two major harmonics. The unstable mode found in the simulation does not have the property of TAE. Thus, we conclude it is not a TAE.

Resonant parallel velocity of energetic ions with the unstable mode is given by $v_\|=\omega R_0/(n-l/q)$ with $l=m,m\pm1$ for substantial energy transfer. We can find a resonance at energetic ion parallel velocity of $0.67v_A$ for $q=1.6$, $l=1$, and $\omega=0.25\omega_A$. The resonant parallel velocity is roughly a half of the NNB injection velocity. For TAE, primary resonant velocity is Alfvén velocity. This is another difference between TAE and the unstable mode found in the simulation.

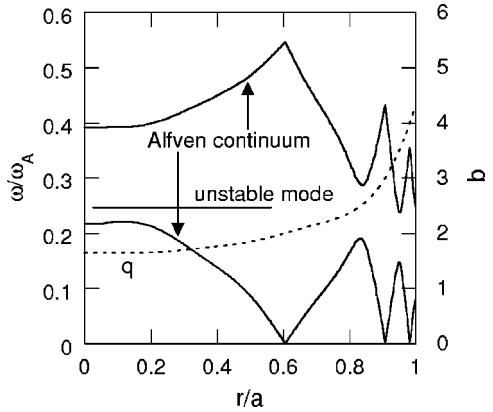

FIG. 3. Frequency and location of the unstable mode. Also shown are the q profile and the shear Alfvén continuous spectra with the toroidal mode number $n=1$.

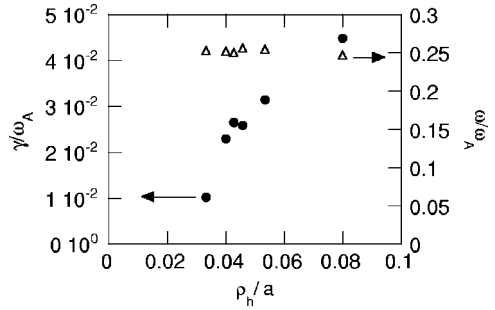

FIG. 4. Growth rate γ and real frequency ω normalized by the Alfvén frequency vs energetic-ion parallel Larmor radius normalized by the minor radius.

B. Effects of energetic-ion orbit width and energetic ion pressure

We have carried out simulations for various energetic-ion orbit widths. Since the energetic-ion orbit width is roughly given by $q\rho_{h\|}$, we solved the extended Grad–Shafranov equation for various $\rho_{h\|}/a$ for initial condition of simulation. Alfvén velocity, major and minor radii, energetic-ion and bulk β values, and energetic ion distribution in the velocity space are kept constant for all of the equilibria. Growth rate and frequency of the unstable mode in the simulation results are shown vs $\rho_{h\|}/a$ in Fig. 4. Instability drive due to energetic ions is in proportion to energetic-ion diamagnetic frequency (e.g., Ref. 33). As the energetic-ion velocity and spatial scale length are kept constant for all of the equilibria, energetic-ion diamagnetic drift frequency is in proportion to $\rho_{h\|}$. Thus, greater $\rho_{h\|}/a$ yields greater growth rate. For $\rho_{h\|}/a=0.02$, no unstable mode was observed. Frequency is roughly constant for all the cases. Peak location and radial width of the unstable mode spatial profile are shown in Fig. 5. Radial width of spatial profile is defined by the region where the total intensity of $m/n=2/1$ harmonic of radial velocity v_r is greater than 10% of the peak value. For greater $\rho_{h\|}/a$, peak location moves radially outward and radial width is broadened. Radial width of the mode spatial profile differs by a factor 3 between the smallest and largest orbit width. Energetic ion orbit width has significant effects on the mode spatial profile. The spatial profile of the unstable mode for the smallest orbit width with $\rho_{h\|}/a=0.033$ is shown in Fig. 6. The spatial profile is extremely localized near the plasma center. The sine component of $m/n=2/1$ harmonic of radial velocity v_r is negligibly small compared to the cosine part. We would like to point out that the q profile shown in Fig. 1 is rather flat at $0<r/a<0.2$. The toroidal MHD effect of second order in inverse aspect ratio[22] might establish the unstable mode in low magnetic shear for small energetic-ion orbit width. The radial width of the unstable mode shown in Fig. 6 gives an upper limit of the radial width of such a purely MHD eigenmode if it does exist.

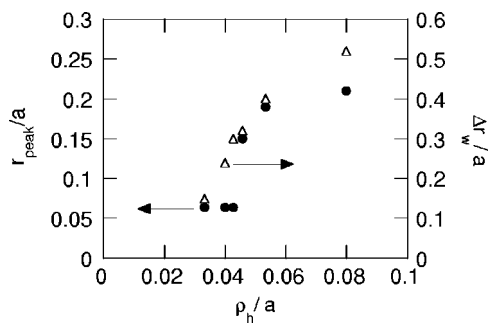

FIG. 5. Peak location r_{peak} and radial width Δr_w of the unstable mode spatial profile vs energetic-ion parallel Larmor radius normalized by the minor radius.

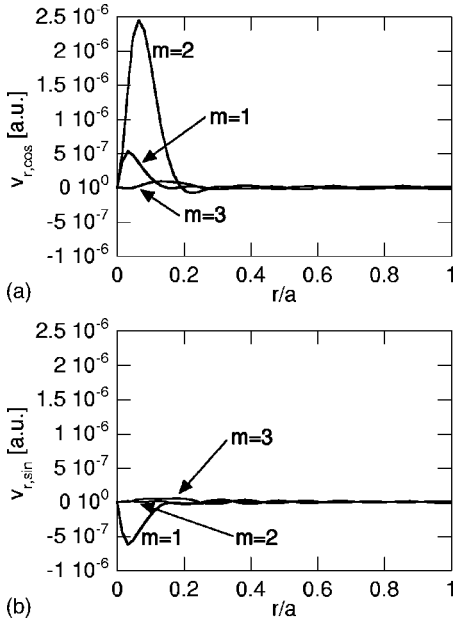

FIG. 6. Spatial profiles of (a) cosine part and (b) sine part of the unstable mode radial velocity v_r harmonics for $\rho_{h\|}/a=0.033$. Toroidal mode number of all the harmonics is $n=1$.

We have investigated radial restoring force in the right-hand side of Eq. (2). The second-order terms in velocity are negligibly small in the linear growth phase. Radial restoring force means a force component in the minor radius coordinate, which contributes to real frequency of the oscillation. The other force component contributes to growth or damping. The MHD force $(=-\nabla p+\mathbf{j}\times\mathbf{B})$ and the energetic-ion force $(=-\mathbf{j}_h\times\mathbf{B})$ are analyzed respectively for various radial location and converted to the real frequency through

$$\omega=(-F_{r\,\cos}v_{r\,\sin}+F_{r\,\sin}v_{r\,\cos})/\rho(v_{r\,\cos}^2+v_{r\,\sin}^2), \tag{30}$$

where F_r denotes the radial MHD force or the radial energetic-ion force. The results are shown in Fig. 7. Figure 7(a) is for $\rho_{h\|}/a=0.08$, which is for the JT-60U plasma, while Fig. 7(b) is for $\rho_{h\|}/a=0.033$. It can be seen in Fig. 7(a) that the total frequency ω_{total} which is the sum of the MHD frequency ω_{MHD} and the energetic-ion frequency $\omega_{energetic}$ takes roughly a constant value in the region $0<r/a<0.5$ where the unstable mode has substantial intensity. The total frequency is close to the frequency of the unstable mode ($\omega=0.25\omega_A$). What is important is that the MHD force alone cannot keep the frequency spatially constant. The energetic-ion frequency amounts to $-0.15\omega_A$, which is about 60% of the unstable mode frequency. The energetic ions have significant effects on the unstable mode oscillation. For $\rho_{h\|}/a$

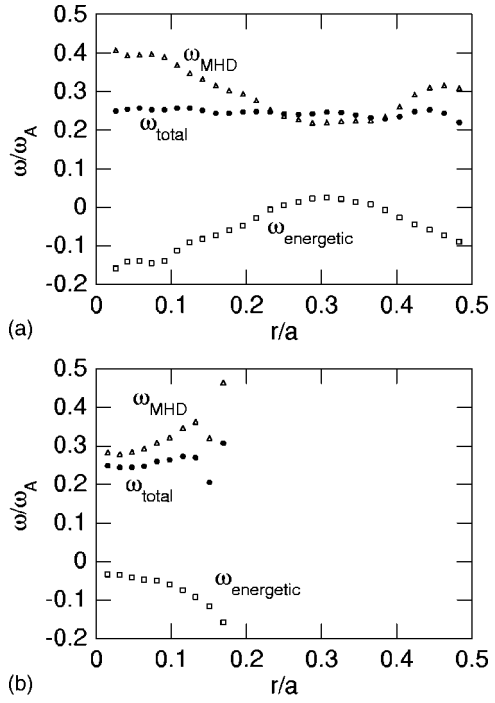

FIG. 7. Frequency profile converted from radial restoring force for (a) $\rho_{h\|}/a=0.08$ and (b) $\rho_{h\|}/a=0.033$. Here, ω_{MHD}, $\omega_{energetic}$, and ω_{total} denote frequency converted from the MHD force, the energetic-ion force, and the total force, respectively.

$=0.033$ the energetic-ion frequency is only 10% of the total frequency near the plasma center. This means that the energetic-ion effects are weak for small orbit width.

We have carried out simulations for various energetic-ion pressures. Compared with the classical energetic-ion β value β_{h0} calculated using the OFMC code, the investigated energetic-ion β values are $\beta_h/\beta_{h0}=0.1$, 0.2, 0.6, and 1.0. For $\beta_h/\beta_{h0}=0.1$, no unstable mode was observed because low energetic-ion pressure leads to small growth rate. Growth rate and frequency in the simulation results are summarized in Fig. 8. The energetic-ion β value in the experiment is lower than the OFMC code calculation result, because the energetic ion loss and redistribution take place in the experiment due to fast FS mode and ALE with time intervals much shorter than the slowing down time. We can see in Fig. 8 that the mode is unstable even when the energetic-ion pressure is

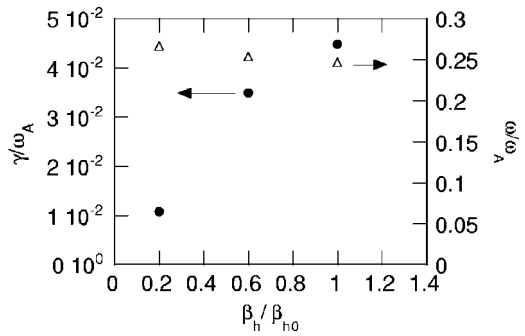

FIG. 8. Growth rate γ and real frequency ω normalized by the Alfvén frequency vs energetic-ion beta value β_h normalized by the classical energetic-ion beta value β_{h0}.

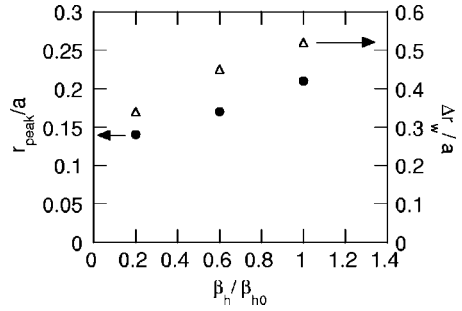

FIG. 9. Peak location r_{peak} and radial width Δr_w of the unstable mode spatial profile vs energetic-ion beta value β_h normalized by the classical energetic ion beta value β_{h0}.

reduced to 1/5 of the classical distribution calculated using the OFMC code. This is qualitatively consistent with actual experimental situation. Peak location and radial width of the unstable mode spatial profile are shown in Fig. 9. Higher energetic-ion pressure moves peak location radially outward and broadens radial width of the unstable mode spatial profile. Energetic-ion pressure has significant effects similar to the energetic-ion orbit width on the unstable mode spatial profile.

IV. SUMMARY

Energetic-ion driven instability in a JT-60U plasma where the fast frequency sweeping mode was observed was investigated using a simulation code for MHD and energetic particles, MEGA. The spatial profile of the unstable mode peaks near the plasma center where the safety factor profile is flat. The unstable mode is not a TAE because the spatial profile deviates from the expected location of TAE and the spatial profile consists of a single primary harmonic $m/n=2/1$, where m and n are poloidal and toroidal mode numbers. The real frequency of the unstable mode is close to the experimental starting frequency of the fast frequency sweeping mode.

Simulations for various energetic-ion orbit widths and energetic-ion pressures were carried out to investigate energetic-ion effects on the unstable mode spatial profile. Both energetic-ion orbit width and energetic-ion pressure broaden radial profile of the unstable mode. Energetic-ion orbit width has significant effects on the mode spatial profile. For the smallest orbit width, the spatial profile is extremely localized near the plasma center where the safety factor profile is rather flat at $0<r/a<0.2$. For larger orbit width, peak location moves radially outward and radial width is broadened. Radial width of the mode spatial profile differs by a factor of 3 between the smallest and the largest (=experimental) orbit width. Radial restoring force, which is a force component in the minor radius coordinate and contributes to real frequency of the oscillation, was analyzed. The MHD force and the energetic-ion force were analyzed for various radial locations and converted to the real frequency. For the largest orbit width, the total frequency which is the sum of the MHD frequency and the energetic-ion frequency takes roughly a constant value in the region $0<r/a<0.5$, where the unstable mode has substantial inten-

sity. The total frequency is close to the frequency of the unstable mode. What is important is that the MHD force alone cannot keep the frequency spatially constant. The energetic-ion frequency amounts to $-0.15\omega_A$, which is about 60% of the unstable mode frequency. The energetic ions have significant effects on the unstable mode oscillation for the largest orbit width. For the smallest orbit width, the energetic-ion frequency is only 10% of the total frequency near the plasma center. This might suggest the existence of a purely MHD eigenmode. However, if such a purely MHD eigenmode does exist without the presence of energetic ions, the spatial profiles of the unstable mode must be independent of the energetic-ion parameters. We cannot find such a parameter region in Fig. 5. Since we cannot investigate instabilities of low growth rate with the initial value approach, theoretical investigations are needed to clarify the existence of a purely MHD eigenmode near the plasma center with low magnetic shear.

The spatial width of the unstable mode with the smallest orbit width gives an upper limit of the spatial width which the MHD effects alone can induce. For the experimental condition of the JT-60U plasma, the energetic ions broaden the spatial profile of the unstable mode by a factor of 3. The major part of the spatial profile of the unstable mode is induced by the energetic ions. We conclude that the unstable mode is primarily induced by the energetic particles and the name "nonlocal EPM"[9] can be justified.

ACKNOWLEDGMENTS

The authors would like to thank Dr. Y. Kusama and Dr. T. Ozeki for valuable advice and continuous encouragement. Numerical computations were performed at the Man-Machine Interactive System for Simulation (MISSION) of National Institute for Fusion Science.

This work was partially supported by Grants in Aid for Scientific Research of the Japan Society for the Promotion of Science (Grant Nos. 14780396 and 16560728).

[1] S. Ishida, JT-60 Team, and JFT-2M Group, Phys. Plasmas **11**, 2532 (2004).
[2] Y. Kusama, G. J. Kramer, H. Kimura *et al.*, Nucl. Fusion **39**, 1837 (1999).
[3] G. J. Kramer, M. Iwase, Y. Kusama *et al.*, Nucl. Fusion **40**, 1383 (2000).
[4] K. Shinohara, Y. Kusama, M. Takechi *et al.*, Nucl. Fusion **41**, 603 (2001).
[5] K. Shinohara, M. Takechi, M. Ishikawa *et al.*, Nucl. Fusion **42**, 942 (2002).
[6] C. Z. Cheng, L. Chen, and M. S. Chance, Ann. Phys. (N.Y.) **161**, 21 (1985).
[7] C. Z. Cheng and M. S. Chance, Phys. Fluids **29**, 3659 (1986).
[8] Y. Todo and T. Sato, Phys. Plasmas **5**, 1321 (1998).
[9] Y. Todo, K. Shinohara, M. Takechi, and M. Ishikawa, J. Plasma Fusion Res. **79**, 1107 (2003), http://jspf.nifs.ac.jp/Journal/2003.html
[10] H. L. Berk, B. N. Breizman, and N. V. Petviashvili, Phys. Lett. A **234**, 213 (1997); **238**, 408(E) (1998).
[11] H. L. Berk, B. N. Breizman, J. Candy, M. Pekker, and N. V. Petviashvili, Phys. Plasmas **6**, 3102 (1999).
[12] L. Chen, Phys. Plasmas **1**, 1519 (1994).
[13] C. Z. Cheng, N. N. Gorelenkov, and C. T. Hsu, Nucl. Fusion **35**, 1639 (1995).
[14] H. L. Berk, D. N. Borba, B. N. Breizman, S. D. Pinches, and S. E. Sharapov, Phys. Rev. Lett. **87**, 185002 (2001).
[15] F. Zonca, S. Briguglio, L. Chen, S. Dettrick, G. Fogaccia, D. Testa, and G. Vlad, Phys. Plasmas **9**, 4939 (2002).
[16] A. Fukuyama and T. Akutsu, *Proceedings of the 19th IAEA Fusion Energy Conference, Lyon, October 2002* (IAEA, Vienna, 2003), TH/P3-14.
[17] K. Appert, R. Gruber, F. Troyon, and J. Vaclavik, Plasma Phys. **24**, 1147 (1982).
[18] D. Borba, H. L. Berk, B. N. Breizman, A. Fasoli, F. Nabais, S. D. Pinches, S. E. Sharapov, and D. Testa, Nucl. Fusion **42**, 1029 (2002).
[19] M. Takechi, A. Fukuyama, K. Shinohara *et al.*, *Proceedings of the 19th IAEA Fusion Energy Conference, Lyon, October 2002* (IAEA, Vienna, 2003), EX/W-6.
[20] M. Takechi, A. Fukuyama, M. Ishikawa *et al.*, "Alfvén eigenmodes in reversed shear plasmas in JT-60U negative-ion-based NBI discharges," Phys. Plasmas (submitted).
[21] R. Nazikian, G. J. Kramer, C. Z. Cheng, N. N. Gorelenkov, H. L. Berk, and S. E. Sharapov, Phys. Rev. Lett. **91**, 125003 (2003).
[22] B. N. Breizman, H. L. Berk, M. S. Pekker, S. D. Pinches, and S. E. Sharapov, Phys. Plasmas **10**, 3649 (2003).
[23] W. Park, S. Parker, H. Biglari, M. Chance, L. Chen, C. Z. Cheng, T. S. Hahm, W. W. Lee, R. Kulsrud, D. Monticello, L. Sugiyama, and R. White, Phys. Fluids B **4**, 2033 (1992).
[24] Y. Todo, T. Sato, K. Watanabe, T. H. Watanabe, and R. Horiuchi, Phys. Plasmas **2**, 2711 (1995).
[25] E. V. Belova, N. N. Gorelenkov, and C. Z. Cheng, Phys. Plasmas **10**, 3240 (2003).
[26] A. M. Dimits and W. W. Lee, J. Comput. Phys. **107**, 309 (1993).
[27] S. E. Parker and W. W. Lee, Phys. Fluids B **5**, 77 (1993).
[28] A. Aydemir, Phys. Plasmas **1**, 822 (1994).
[29] R. Nazikian, G. Y. Fu, S. H. Batha *et al.*, Phys. Rev. Lett. **78**, 2976 (1997).
[30] Y. Chen, R. B. White, G. Y. Fu, and R. Nazikian, Phys. Plasmas **6**, 226 (1999).
[31] G. Y. Fu, R. Nazikian, R. Budny, and Z. Chang, Phys. Plasmas **5**, 4284 (1998).
[32] K. Tani, M. Azumi, H. Kishimoto, and S. Tamura, J. Phys. Soc. Jpn. **50**, 1726 (1981).
[33] G. Y. Fu and J. W. Van Dam, Phys. Fluids B **1**, 1949 (1989).